Available online at www.sciencedirect.com
ScienceDirect
International Journal of Thermal Sciences 45 (2006) 1166–1178
International Journal of Thermal Sciences
www.elsevier.com/locate/ijts

Convective heat transfer inside a rotating cylinder with an axial air flow

S. Seghir-Ouali [a,c,*], D. Saury [a], S. Harmand [a,c], O. Phillipart [b], D. Laloy [b,c]

[a] *Laboratoire de Mécanique et Energétique, Université de Valenciennes et du Hainaut-Cambrésis, Le Mont Houy, 59313 Valenciennes cedex 9, France*
[b] *FRAMATOME-ANP/Jeumont, F59573 Jeumont, BP 189, France*
[c] *Centre National de Recherche Technologique, FUTURELEC 2, France*

Received 7 September 2005; received in revised form 16 January 2006; accepted 19 January 2006

Available online 20 March 2006

Abstract

This article presents an experimental identification technique for the convective heat transfer coefficient inside a rotating cylinder with an axial airflow. The method consists in heating the outer face of the cylinder using infrared lamps, and acquiring the evolution of the external surface temperature versus time using an infrared camera. Heat transfer coefficients are identified via three methods. The first one is based on an inverse model, the second one assumes the wall of the cylinder as a thermally thin wall and the third one is based on an analytical method permitting to obtain the temperature field within the whole cylinder. The experiments were carried out for a rotational speed ranging from 4 to 880 rpm corresponding to rotational Reynolds numbers varying from 1.6×10^3 to 4.7×10^5 and an air flow rate varying from 0 to 530 $m^3\,h^{-1}$ which corresponds to an axial Reynolds numbers ranging from 0 to 3×10^4. Correlations connecting the Nusselt number to the axial and rotational Reynolds numbers are also proposed.

Keywords: Convective heat transfer; Rotating machine; Infrared thermography; Identification method

1. Introduction

Rotating electric machines are subject to very severe heating phenomena resulting from electric losses occurring in their different constituents. To maintain the proper use of a motor it is therefore necessary to have perfectly designed cooling systems. In the absence of cooling, materials used are unable to sustain the temperature levels obtained during use without serious damage. Heating problems within these machines remain alarming despite progress made these last few years as regards their design. In order to avoid or minimize these overheating phenomena, cooling systems allowing the dissipation of the heat flux towards the ambient surrounding have to be taken into account in the optimized design of such machines.

In order to significantly decrease the temperature within the rotating part (rotor), it is essential to have a correct idea of the heat transfer between the rotor surface and the air in contact with it. The most usual rotor geometry is a full cylindrical rotor placed inside a fixed stator. For such configurations flows onto the external face of the rotor are widely studied with for instance the flows of Taylor–Couette [1–3] or Couette–Poiseuille [4,5].

However, the case where an empty cylinder is used as a rotor is less documented in literature and there only exist few correlations to obtain the convective heat exchange on the inner face. This study aims at experimentally identifying the heat transfer coefficients within a rotating empty cylinder with an internal axial airflow. The experimental procedure is based on the measurement of the heated cylinder surface temperature evolution versus time using infrared thermography. The heat transfer coefficient is then identified by resolving the heat equations using three different methods: an analytical solution of the heat equation, an inverse technique and a global heat balance with the assumption of a thermally thin wall.

* Corresponding author. Tel.: + 33 327 511 971; fax: + 33 327 511 961.
E-mail address: souhil.seghir-ouali@meletu.univ-valenciennes.fr (S. Seghir-Ouali).

1290-0729/$ – see front matter
doi:10.1016/j.ijthermalsci.2006.01.017

Nomenclature

a	thermal diffusivity, $= \lambda/\rho c$	$m^2\,s^{-1}$
Bi	Biot number, $= eh/\lambda$	
c	specific heat	$J\,kg^{-1}\,K^{-1}$
D	cylinder diameter	m
e	cylinder wall thickness	m
g	gravity, $= 9.81$	$m\,s^{-2}$
Gr	Grashof number, $= g\beta(T_p - T_\infty)D_e^3/\nu^2$	
h	heat transfer coefficient	$W\,m^{-2}\,K^{-1}$
H	$= h/\lambda$	m^{-1}
I	thermal level	
ℓ	bridle thickness	m
L	length of rotating test section	m
m	mass of the test section	kg
Nu	Nusselt number, $= Dh/\lambda$	
Pr	Prandtl number, $= \mu c/\lambda$	
Q_v	air flow rate	$m^3\,h^{-1}$
r	radius of cylinder	m
Re_a	axial Reynolds number, $= 4Q_v/\pi\nu D_i$	
Re_r	rotational Reynolds number, $= \omega D_i^2/2\nu$	
S	surface or section	m^2
t	time	s
Δt	time step	s
T	temperature	K
U	velocity	$m\,s^{-1}$
	or voltage	V
x	abscissa in the thickness of cylinder direction	m
Δx	space step	m
z	axial coordinate	m

Greek symbols

α	angle	rad
β	thermal coefficient of volumetric expansion	K^{-1}
ε	emissivity/relative error	
φ	heat flux density	$W\,m^{-2}$
φ_0	IR lamps heat flux density	$W\,m^{-2}$
λ	thermal conductivity	$W\,m^{-1}\,K^{-1}$
μ	dynamic viscosity	$kg\,m^{-1}\,s^{-1}$
ν	kinematic viscosity	$m^2\,s^{-1}$
ρ	density	$kg\,m^{-3}$
ω	rotational speed	$rad\,s^{-1}$
σ	Stefan–Boltzmann constant, $= 5.67 \times 10^{-8}$	$W\,m^{-2}\,K^{-4}$
θ	temperature difference	K
χ	$= (\Delta x)^2/(a\Delta t)$	

Subscripts and superscripts

a	axial
c	critical
corr	correlation
cv	convection
cyl	cylinder
e	exterior
exp	experiment
i	interior
max	maximal
nc	free convection
p	wall
r	rotational/radiation
VT	vetronite epoxy
∞	ambient

2. Literature survey

2.1. Convective heat transfer from a horizontal rotating cylinder

Convective heat transfer from a horizontal rotating cylinder has been studied by many authors. Most of them concluded that rotation has no significant effects on the heat transfer coefficient for low rotational speeds and that the heat transfer is governed by free convection.

However, for very high rotational speeds, the forced convection is the preponderant heat transfer regime and the average Nusselt number on the cylinder surface is often obtained with correlations such as $Nu = a\,Re^b$ (a and b being constants whose values vary from one author to another). Between the free and forced convection regimes, there is a transitional phase, which corresponds to the mixed convection regime and where the average Nusselt number depends on both the Reynolds and Grashof numbers. Correlations found by the main authors about the convective heat transfer for a horizontal rotating cylinder have been gathered on Table 1.

2.2. Heat transfer coefficient inside a stationary cylinder

Study about convective heat transfer inside stationary tubes was carried out by many authors, for numerous geometries and various flow types. In the case of stationary tubes with an axial flow, the Dittus and Boelter correlation can for instance be quoted [16–19]:

$$Nu = 0.023 Pr^{0.4} Re_a^{0.8} \tag{13}$$

This correlation is used for long and/or low diameter tubes since it remains valid for a length/diameter ratio greater than 60. The Prandtl number has to range between 0.7 and 120 and the axial Reynolds number must be ranging between 10^4 and 1.2×10^5.

Colburn [17,20] proposes the following correlation, also valid for a $L/D > 60$ ratio, a Prandtl number ranging from 0.7 to 100 and an axial Reynolds number between 10^4 and 1.2×10^5:

$$Nu = 0.023 Pr^{1/3} Re_a^{0.8} \tag{14}$$

Table 1
Heat transfer correlation from rotating cylinder

Authors	Validity criteria	Correlation	
Morales et al. [6]	$1 \leqslant [Gr/(Re^2)]$ and $1.42 \times 10^4 < Gr < 1.42 \times 10^8$	$Nu = Nu_{nc} - 2.345 \times 10^{-8} Gr\,[Gr/Re^2]^{-0.783}$	(1)
Anderson and Saunders [7]	$Re > Re_c = 1.09 Gr^{0.5}$	$Nu = 0.1 Re^{0.66}$	(2)
Etemad [8]	$1000 < Re < 8000$	$Nu = 0.11\,[(0.5Re^2 + Gr) \times Pr]^{0.35}$	(3)
	$8000 < Re < 65\,400$	$Nu = 0.076 Re^{0.7}$	(4)
Dropkin and Carmi [9]	$0 < Re < 2500$	$Nu = 0.095\,[0.5Re^2 + Gr]^{0.35}$	(5)
	$15\,000 < Re < 433\,000$	$Nu = 0.073 Re^{0.7}$	(6)
Kays and Bjorklund [10]	$600 < Re < 50\,000$	$Nu = 0.095 Re^{0.66}$	(7)
Abu-Hijleh and Heilen [11]	$5 < Re < 450$ and $0.1 < k = Gr/Re^2 < 10$	$Nu = 1.586 + 0.051 Re^{0.7072} \times A$ $A = [-0.4497 + 2.254 k^{0.6729}]^{0.5978}$	(8)
Becker [12]	$800 < Re < 10^5$	$Nu = 0.133 Re^{2/3} Pr^{1/3}$	(9)
Kendoush [13]	$10^3 < Re < 10^4$	$Nu = 0.6366\,[Re\,Pr]^{0.5}$	(10)
Özerdem [14]	$2000 < Re < 40\,000$	$Nu = 0.318 Re^{0.571}$	(11)
Shimada et al. [15]	$300 < Re < 3000$	$Nu = 0.046\,[Re^2 + 8Gr]^{0.35}$	(12)

Later on, McAdams [21] proposes the correlation taking into account the L/D ratio:

$$Nu = 0.023 Pr^{1/3} Re_a^{0.8} \left[1 + \left(\frac{D}{L}\right)^{0.7}\right] \tag{15}$$

This correlation remains valid for a Prandtl number ranging from 0.7 to 100, a Reynolds number ranging from 10^4 to 1.2×10^5. For this correlation, the L/D aspect ratio must remain between 2 and 20.

In transitional regime ($2300 < Re_a < 8000$), Hausen [22] proposes this correlation:

$$Nu = 0.016 Pr^{0.33} \left(Re_a^{0.66} - 125\right) \left[1 + \left(\frac{D}{L}\right)^{0.66}\right] \tag{16}$$

For laminar $Re_a < 2300$ regime, Hausen [22–24] also proposes the following correlation, obtained for aspect L/D ratios equal to 0.5, 0.1, and 0.01:

$$Nu = 3.66 + \frac{0.0668 Re_a Pr\, D/L}{1 + 0.04 (Re_a Pr\, D/L)^{0.667}} \tag{17}$$

Many other correlations can be found in literature for this type of configuration and this list is far from being exhaustive.

2.3. Fluid flow and heat transfer in a rotating cylinder with an internal axial airflow

The flow and the heat transfer inside an empty cylinder rotating around its axis and subjected to an axial airflow have aroused a certain interest for a few decades now. This configuration has been investigated with numerous experimental, theoretical and numerical studies where many authors studied the influence of rotation on the flow structure and the heat transfer.

Whenever a flow enters through a rotating cylinder, tangential forces taking place between the wall of the rotating cylinder and the fluid drive the fluid in rotation with the cylinder resulting in a flow pattern rather different from the one observed within a stationary cylinder. Pedley [25] was one of the first authors to probe the Hagen–Poiseuille. Flow becomes unstable with an infinitesimal disturbance when the cylinder rotates around its axis. These results have been experimentally confirmed by Nagib et al. [26]. Mackrodt [27] studied the stability of the Hagen–Poiseuille flow through a rotating cylinder. Using numerical solutions of the movement equations, he found critical values from which the flow becomes unstable.

Effects of the cylinder rotation on the charge loss have been experimentally investigated by Levy [28], White [29] and Shchukin [30]. If the flow is initially turbulent, the pressure loss decreases with the increase in the rotational speed when compared to the pressure loss of a static cylinder.

For turbulent flows through a rotating cylinder, Borisenko et al. [31] analysed the effect of rotation on the turbulent fluctuations of the velocity using hot-wire probes. They showed turbulent effects disappeared when the rotational speed increases. Murakami and Kikuyama [32] in an experimental study showed that the cylinder rotation entails an attenuation of the turbulence effects in the axial flow. With the increase in the rotational speed, the axial velocity distribution tends towards the Hagen–Poiseuille flow. Kikuyama et al. [33] experimentally and theoretically demonstrated using a modified mixing length theory that in the case of a turbulent axial flow in a rotating cylinder, the rotation tends to have a laminar flow. On the other hand, they found a destabilizing effect for the flow due to the rotation when the inlet flow is laminar. According to Murakami et al. [34], in the case of an undeveloped flow in a rotating cylinder, the cylinder rotation entails two opposite effects on the developing dynamic boundary layer: a destabilizing effect due to an increase in the fluid velocity at the surface of the rotating cylinder and a stabilizing effect due to the turbulence suppression caused by the centrifugal force. Kikuyama et al. [35] measured the mean velocities and turbulent fluctuations inside the developed boundary layers. Authors showed that the cylinder rotation entailed two opposite effects on the flow: a destabilizing effect

due to an increase in the shear stress caused by the wall rotation near the inlet area of the rotating cylinder, and a stabilizing effect due to the centrifugal force, which becomes predominant in the area far from the inlet. Imao et al. [36] carried out an experimental analysis on the turbulent characteristics of a fully developed flow in a rotating cylinder using Laser Doppler Velocimetry (LDV). Their results indicate that turbulent fluctuations in the rotating cylinder gradually decrease when cylinder rotation increases.

There are but few works about the identification of the convective heat transfer. Among these studies, the authors [37,38] showed the rotation of the cylinder has a destabilizing effect on the laminar flow which becomes turbulent, entailing a higher heat transfer rate between the cylinder and the airflow. Other authors [39–41] conclude that the cylinder rotation reduces the heat transfer rate if the flow is initially turbulent.

Reich [37] observed the building up of convection cells in a heated cylinder for low flow rates and a $Gr/Re_a^2 \approx 0.02$ ratio. The rotation of the cylinder around its axis causes the disappearance of these convection cells. Reich et al. [38] pointed out that the rotation has a destabilizing effect on laminar flows and enhance the heat transfer rate between the cylinder and the flow. Free convection cells appearing if the cylinder wall is heated disappear whenever the cylinder rotational speed increases. Cannon and Kays [39] showed that the most noticeable influence is observed in the transition from laminar to turbulent flow. When the axial flow becomes turbulent, the convective heat transfer becomes insensitive to rotation. A visualization of the flow revealed that cylinder rotation tends to stabilize laminar flow to such a degree that transition appears for higher axial Reynolds numbers. Reich and Beer [40] carried out an experimental and analytical study. The analytical study is performed for flow and heat transfer in a rotating cylinder using a modified mixing length theory. The cylinder rotation (and thus the presence of the centrifugal forces radially increasing) plays a pivotal part on the decrease in the turbulence and thus entails a reduction in the heat transfer rate. Weigand and Beer [41] theoretically studied the effects of cylinder rotation on the heat transfer with a fluid flowing inside a cylinder. The cylinder rotation causes a decrease in heat transfer. When the rotation rate tends towards infinity, the Nusselt number tends towards the value of the Nusselt number for laminar flow in a static cylinder.

However it was observed that these studies cover a relatively limited field since they are only valid for high values of the geometrical aspect ratios L/D. Results available in the literature do not allow to find out trends and correlations connecting the Nusselt numbers to the axial and rotational Reynolds numbers.

3. Experimental setup

3.1. Experimental principle

This study aims at identifying the convective heat transfer coefficient in an empty cylinder rotating around its axis with an inner axial air flow. The temperature on the outer face of the heated cylinder is obtained using infrared thermography. The heat equation in the cylinder is solved with three different methods permitting to obtain the internal convective heat transfer coefficient. This resolution uses boundary and initial conditions imposed by experiments.

3.2. Experimental setup description

Fig. 1 presents the experimental setup. The rotating part is composed of three cylinders made of steel and separated by a vetronite epoxy (VT) insulation whose conductivity λ_{VT} is 0.3 $W\,m^{-1}\,K^{-1}$. These cylinders are concentric and reamed together to obtain a perfect inner surface quality. The 198 mm long central cylinder corresponds to the test section. The inner and outer diameters of the cylinders under study are respectively 393 and 403 mm. The two 330 mm long cylinders surrounding the central cylinder (test section) are used to avoid parasitic phenomena at their inlet and outlet, the insulation in VT being used to minimize the heat losses from the studied zone towards the two connection cylinders. The external face of the test section is heated with two fixed infrared transmitters located above and below the rotating part and connected to a power regulator. The power supply to the heat transmitters can be regulated manually between 0 and 4 kW. An electric motor associated to a variable speed transmission drives the cylinder up to 1000 rpm. The rotating part is connected to the static part with two ball bearings assembled into ball self-aligning bearings.

The static part is composed of a centrifugal ventilator connected to the revolving part with a 1.3 m long pipe on which a diaphragm is placed. The fan imposes an air flow in the test bench from 0 to about 530 $m^3\,h^{-1}$. Upstream and downstream the diaphragm, two pressure tappings are placed, measuring the air flow rate flowing in the setup. The airflow generated by the fan to the revolving part impacts on a flask tapped with 4 holes, 50 mm wide, and equally distributed. The impact zone is in a small plenum chamber. The air from the fan goes into the rotating part via the plenum chamber, flows through the first connection cylinder used to homogenize the velocity profiles, then it flows through the test area, and finally through the last connection cylinder before flowing by the outlet flask which is identical to the inlet flask.

3.3. Heat flux measurement and heating power estimation

The infrared lamps are connected to a regulator controlling the heat power transmitted to the cylinder. For each imposed power step, the heat flux received by the cylinder is identified versus the α angle (versus a horizontal line) using the radiative heat flux sensors noted CF_i on Fig. 2(a). These sensors are placed on the external surface of the zone studied and equally distributed in the axial direction (cf. Fig. 2(a)). These square radiative heat flux sensors are sensitive neither to the conduction nor to the convection phenomena. They are 10 mm wide and 300 μm thick. Their response time is about 100 ms and they have a linear sensitivity to the heat flux of about 0.5 mV ($W^{-1}\,m^2$). Relative uncertainty on the

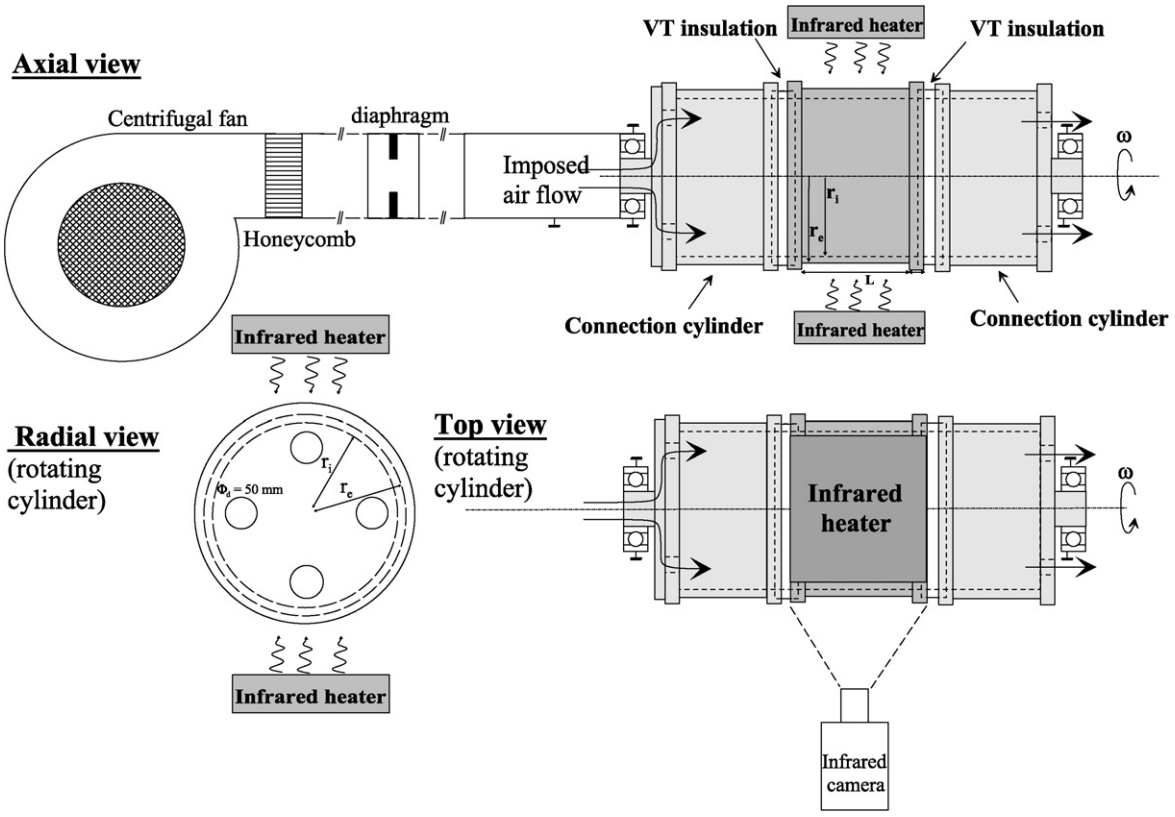

Fig. 1. Scheme of the experimental setup.

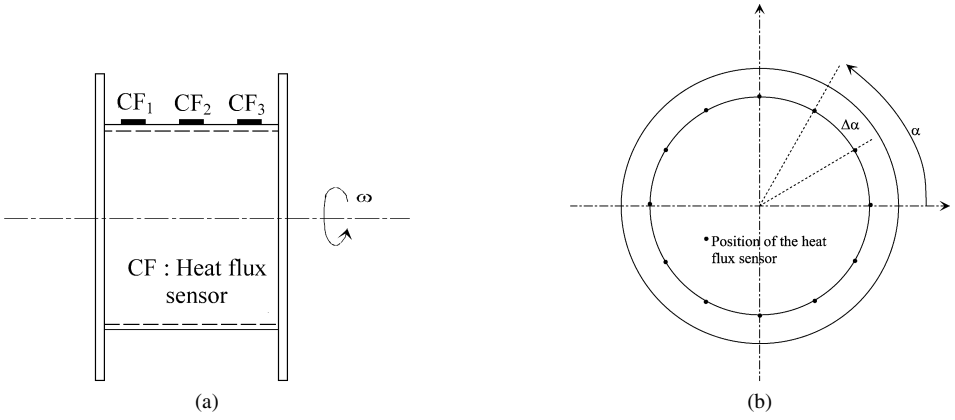

Fig. 2. (a) Position of the heat flux sensor (axial view); (b) Position of the heat flux sensor (radial view).

heat flux density φ depends directly on the voltage measured since, if s is the sensitivity of the sensor, $\varphi = U/s$ and thus $(\Delta\varphi)/\varphi = (\Delta U)/U \approx 0.5\%$. These sensors carry out a radiative heat balance on the irradiated surface. To know the heat flux density supplied by the infrared lamps φ_0, it will be thus necessary to add to the heat flux density measured with the sensors the part of heat flux emitted by the surface towards the surrounding $(= \varepsilon\sigma(T_p^4 - T_\infty^4))$. The integration of the heat flux density with z and α determines the average heat flux density received by the cylinder since:

$$\varphi_0 = \frac{1}{S}\int_S \varphi \,\mathrm{d}S = \frac{1}{2\pi r_e L}\iint \varphi(z,\alpha) r_e \,\mathrm{d}z\,\mathrm{d}\alpha \tag{18}$$

For example, in nominal use of the infrared transmitters the mean heat flux density received by the cylinder and generated by the IR lamps is $2745 \pm 15\ \mathrm{W\,m^{-2}}$.

3.4. Temperature measurement

The surface temperature is obtained using an infrared camera placed in front of the area under study. It is a short wavelength infrared camera (2–5.4 μm) equipped with $20 \times 12.5°$ lens. It was used with a 20 hertz image acquisition frequency and a 204×128 pixel image definition. Its thermal resolution is 0.1% at 30 °C. This camera returns a signal $I(T)$ for a black body surface at the temperature T observed through a transparent environment. During measurement, the camera re-

turns a digital signal originating from an elementary cylinder surface. In reality, due to the partial transmission through the surrounding air, the signal received by the camera is attenuated. In addition, this signal also takes into account environment radiation which reflects itself onto the cylinder. In order to improve the part of radiative heat flux emitted by the cylinder, the latter is painted black in order to increase its emissivity. The black painted surface emissivity, determined by calibration, is then 0.93 ± 0.02. A second calibration allows to connect, in a real situation, the thermal level I to the real temperature of the cylinder external surface. Absolute uncertainty on the temperature measurement with the camera remains lower than ± 0.1 K for the measurement range. The ambient air temperature, taken as a temperature reference to evaluate the heat transfer coefficient is measured using a type K thermocouple. The diameter of this thermocouple is 0.3 mm and its precision is ± 1 K.

3.5. Air flow rate measurement

A diaphragm placed on the tube (Fig. 1) and the two pressure taps placed upstream and downstream this diaphragm indicate the flow rate flowing into the cylinder. This diaphragm is calibrated and the law obtained is in good agreement with Idel'cik [42]. It determines this flow rate with a relative uncertainty remaining lower than 6%.

4. Identification models of the internal convective coefficient

4.1. Modeling of the thermal behavior of an empty cylinder

Fig. 3 presents the problem studied. The rotating cylinder is heated on its external face by a radiative heat flux whereas its internal face is cooled down by an airflow whose speed U_∞ and temperature T_∞ are uniform. Initially the cylinder temperature is also assumed to be uniform. The test area is insulated from the other parts of the cylinder to promote a radial heat transfer and to significantly limit the axial and orthoradial heat transfers. In this case the temperature field within the cylinder is supposed to be unidimensional and is denoted by $T(r,t)$. The convective heat transfer between the air and internal and external surfaces is characterized by the total heat transfer coefficients h_i and h_e. On the external surface of the cylinder, the total heat transfer coefficient $h_e = h_e^{cv} + h_e^r$ is defined using the convective and the radiative heat transfer coefficients.

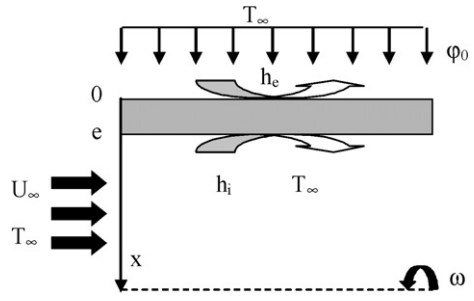

Fig. 3. Scheme of the problem under study.

All thermophysical properties ρ, c and λ of the cylinder are considered constant. Taking into account the relative thinness of the cylinder when compared to its diameter ($e/D = 0.0127$) and defining $\theta(x,t) = T(x,t) - T_\infty$, the temperature evolution in the cylinder is then governed by the following equations:

$$\begin{aligned}
&\frac{1}{a}\frac{\partial\theta(x,t)}{\partial t} = \frac{\partial^2\theta(x,t)}{\partial x^2}\\
&\left.\frac{\partial\theta(x,t)}{\partial x}\right|_{x=0} = H_e\theta(0,t) - \frac{\varphi_0}{\lambda}\\
&\left.\frac{\partial\theta(x,t)}{\partial x}\right|_{x=e} = -H_i\theta(e,t)\\
&\theta(x,0) = \theta_\infty
\end{aligned} \tag{19}$$

Where $H = \frac{h}{\lambda}$ is the ratio between the convection coefficient and the thermal conductivity.

The heat transfer equation and the boundary conditions of the problem define a system of differential equations where unknown quantities are the temperature and the internal convective coefficient h_i. The experimental setup lets determine the temperature evolution of external surface of the cylinder versus time and the heat flux density φ_0. The external convective coefficient h_e is evaluated using data from literature. Then an identification method letting identify the internal convective coefficient have to be developed. Three methods are proposed in this work: thin wall assumption model, inverse method, and analytical resolution of the heat transfer equation.

4.2. Thin wall assumption model

Considering the limited thickness of the wall (5 mm) and the thermal conductivity of the cylinder ($\lambda_{cyl} = 43$ W m^{-1} K^{-1}), the cylinder can be considered at every moment and for certain tests isotherm. With this assumption, the conservation of the energy equation within the cylinder follows the law of the thin bodies, which is written:

$$mc\frac{\mathrm{d}\theta}{\mathrm{d}t} = S_e\varphi_0 - (h_eS_e + h_iS_i)\theta \tag{20}$$

From this relation, the evolution of h versus time is obtained:

$$h_i = \frac{S_e\varphi_0 - mc\frac{\mathrm{d}\theta}{\mathrm{d}t}}{S_i\theta} - h_e\frac{S_e}{S_i} \tag{21}$$

In this equation, $\mathrm{d}\theta/\mathrm{d}t$ is estimated to use the smoothed experimental temperature profile, φ_0 is measured as described in part 3.3, $h_e = h_e^{cv} + h_e^r$ where h_e^{cv} is obtained using the correlation presented in part 2.1 and h_e^r using a linearization of the radiative heat flux, i.e. $h_e^r = \varepsilon\sigma(T_p^2 + T_\infty^2)(T_p + T_\infty)$. In a steady state, the relative uncertainty on h_i obtained with this method and our experimental conditions can easily be determined and remain lower than 6.4%.

4.3. Inverse model

This method consists in an approach based on the finite differences which implies a discretization of the domain. The calculation domain is composed by a network of nodes in which

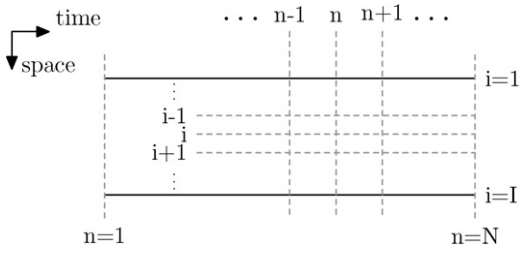

Fig. 4. Spatial and time discretization scheme.

the temperature is calculated. The calculation of the internal convective heat transfer coefficient is achieved in three different steps. The first step consists in calculating the temperature at the point $i = 2$ using a heat balance in the cell between the point of external surface $i = 1$ and the first inner point $i = 2$ (cf. Fig. 4). The measurement point $i = 1$ has two known conditions: its temperature resulting from infrared thermography and the heat flux balance (heating + convection + radiation). In the second step the temperatures in the nodes $i = 3$ to $i = I$ are determined using the heat equation discretization. The third step consists in calculating the convective heat transfer coefficient on the inner surface of the cylinder using the temperature field calculated and the inner surface heat flux balance. For this model, several discretization schemes are used but only the Euler scheme is developed hereafter.

This scheme uses an implicit formulation of the heat balance, thus:

$$\begin{aligned}
&\rho c\frac{\theta_1^{n+1}-\theta_1^n}{\Delta t}=\frac{\varphi_{1+1/2}^{n+1}-\varphi_1^{n+1}}{\Delta x/2} \quad \text{for } i=1\\
&\rho c\frac{\theta_i^{n+1}-\theta_i^n}{\Delta t}=\frac{\varphi_{i+1/2}^{n+1}-\varphi_{i-1/2}^{n+1}}{\Delta x} \quad \text{for } 1<i<I\\
&\rho c\frac{\theta_I^{n+1}-\theta_I^n}{\Delta t}=\frac{\varphi_I^{n+1}-\varphi_{I-1/2}^{n+1}}{\Delta x/2} \quad \text{for } i=I
\end{aligned} \tag{22}$$

The heat flux densities can be formulated like below:

$$\begin{aligned}
&\varphi_{1+1/2}^{n+1}=\lambda\frac{\theta_1^{n+1}-\theta_2^{n+1}}{\Delta x}, \qquad \varphi_1^{n+1}=\varphi_0-h_e\theta_1^{n+1}\\
&\varphi_{i+1/2}^{n+1}=\lambda\frac{\theta_i^{n+1}-\theta_{i+1}^{n+1}}{\Delta x}, \qquad \varphi_{i-1/2}^{n+1}=\lambda\frac{\theta_{i-1}^{n+1}-\theta_i^{n+1}}{\Delta x}\\
&\varphi_I^{n+1}=h_i\theta_I^{n+1}, \qquad \varphi_{I-1/2}^{n+1}=\lambda\frac{\theta_{I-1}^{n+1}-\theta_I^{n+1}}{\Delta x}
\end{aligned} \tag{23}$$

And then, we obtain:

$$\begin{aligned}
&\theta_2^{n+1}=\left[\frac{\Delta x h_e}{\lambda}-\frac{\chi}{2}+1\right]\theta_1^{n+1}+\frac{\chi}{2}\theta_1^n-\frac{\Delta x\varphi_0}{\lambda}\\
&\theta_{i+1}^{n+1}=(2-\chi)\theta_i^{n+1}-\theta_{i-1}^{n+1}+\chi\theta_i^n\\
&h_i=\frac{\rho c\Delta x}{2\Delta t}\frac{\theta_I^{n+1}-\theta_I^n}{\theta_I^{n+1}}+\frac{\lambda}{\Delta x}\frac{\theta_{I-1}^{n+1}-\theta_I^{n+1}}{\theta_I^{n+1}}
\end{aligned} \tag{24}$$

with $\chi=\frac{(\Delta x)^2}{a\Delta t}$, $x_1 = 0$ and $x_I = e$.

The resolution of this system requires the use of θ_1 provided at every moment by the infrared camera. It also requires the knowledge of φ_0 obtained using the heat flux sensors as described in part 3.3. The convective coefficient on the external face (h_e^{cv}) is determined using the correlation of the literature given by Eq. (6) and $h_e^r=\varepsilon\sigma(T_p^2+T_\infty^2)(T_p+T_\infty)$. In a steady state, the relative uncertainty on h_i obtained with this method and with our experimental conditions remains lower than 7.4%.

4.4. Analytical model: Resolution of the heat equation

The development of the theoretical model is performed using an unidirectional modelling of the cylinder thermal behaviour. In addition, the cylinder is assumed to be a flat plate. The system (19) is not homogeneous due to the boundary conditions at $x = 0$. However, its resolution is possible by splitting it into two subsystems and defining θ such as $\theta(x,t)=\theta_A(x,t)+\theta_B(x,t)$. In this last expression, $\theta_A(x,t)$ stands for the solution of the non-stationary homogeneous system, whereas $\theta_B(x)$ is the solution of the non-homogeneous stationary system.

Non-stationary homogeneous subsystem

$$\begin{aligned}
&\frac{1}{a}\frac{\partial\theta_A(x,t)}{\partial t}=\frac{\partial^2\theta_A(x,t)}{\partial x^2}\\
&\left.\frac{\partial\theta_A(x,t)}{\partial x}\right|_{x=0}=H_e\theta_A(0,t)\\
&\left.\frac{\partial\theta_A(x,t)}{\partial x}\right|_{x=e}=-H_i\theta_A(e,t)\\
&\theta_A(x,0)=-\theta_B(x)
\end{aligned} \tag{25}$$

Stationary subsystem

$$\begin{aligned}
&\frac{\partial^2\theta_B(x)}{\partial x^2}=0\\
&\left.\frac{\partial\theta_B(x)}{\partial x}\right|_{x=0}=H_e\theta_B(0)-\frac{\varphi_0}{\lambda}\\
&\left.\frac{\partial\theta_B(x)}{\partial x}\right|_{x=e}=-H_i\theta_B(e)
\end{aligned} \tag{26}$$

The resolution of the stationary subsystem (26) provides:

$$\theta_B(x)=-\frac{\varphi_0}{\lambda[1+\frac{H_e}{H_i}(1+H_ie)]}\left[x-\frac{(1+H_ie)}{H_i}\right] \tag{27}$$

The solution of the homogeneous non-stationary subsystem (25) is obtained using the variable separation method. This solution appears as:

$$\theta_A(x,t)=e^{-ak^2t^2}\left[\gamma\cos(kx)+\delta\sin(kx)\right] \tag{28}$$

Where the K, γ and δ parameters have to satisfy the boundary conditions.

The boundary conditions in $x = 0$ and $x = e$ are:

$$\begin{aligned}
&x=0\text{: } k\delta=H_e\gamma\\
&x=e\text{: } k\left(-\gamma\sin(ke)+\delta\cos(ke)\right)\\
&\qquad=-H_i\left(\gamma\cos(ke)+\delta\sin(ke)\right)
\end{aligned}$$

By combining both equations, the following transcendent equation is obtained:

$$\mathrm{tg}(ke)\left[Bi_e Bi_i - (ke)^2\right] = -ke(Bi_e + Bi_i) \tag{29}$$

This characteristic equation admits an infinity of discrete solutions k_n. The roots of this equation depend on the values of the external and internal Biot numbers ($Bi_e = eH_e$ and $Bi_i = eH_i$). The general solution of the system (25) is expressed as a series by:

$$\theta_A(x,t) = \sum_{n=1}^{\infty} e^{-ak_n^2 t}\left[\gamma_n \cos(k_n x) + \delta_n \sin(k_n x)\right] \tag{30}$$

Constants γ_n and δ_n must satisfy the initial condition:

$$\theta_A(x,0) = -\theta_B(x) = \sum_{n=1}^{\infty}\left[\gamma_n \cos(k_n x) + \delta_n \sin(k_n x)\right] \tag{31}$$

Applying the Fourier series theory, we obtained:

$$\gamma_n = -\frac{\int_0^e \cos(k_n x)\theta_B(x)\,\mathrm{d}x}{\int_0^e \cos^2(k_n x)\,\mathrm{d}x}$$

$$\delta_n = -\frac{\int_0^e \sin(k_n x)\theta_B(x)\,\mathrm{d}x}{\int_0^e \sin^2(k_n x)\,\mathrm{d}x}$$

After integration γ_n and δ_n are:

$$\gamma_n = \frac{2k_n\psi}{\cos(k_n e)\sin(k_n e) + ek_n} \times \left[\frac{e-\phi}{k_n}\sin(k_n e) + \frac{1}{k_n^2}\cos(k_n e) - \frac{1}{k_n^2}\right] \tag{32}$$

$$\delta_n = \frac{2k_n\psi}{ek_n - \cos(k_n e)\sin(k_n e)} \times \left[\frac{\phi-e}{k_n}\cos(k_n e) + \frac{1}{k_n^2}\sin(k_n e) - \frac{\phi}{k_n}\right] \tag{33}$$

With $\psi = \frac{\phi_0}{\lambda[1+\frac{H_e}{H_i}(1+H_i e)]}$ and $\phi = \frac{(1+H_i e)}{H_i}$.

Finally, the solution of the coupled problem is written:

$$\theta(x,t) = \sum_{n=1}^{\infty} e^{-ak_n^2 t}\left[\gamma_n \cos(k_n x) + \delta_n \sin(k_n x)\right] - \frac{\varphi_0}{\lambda[1+\frac{H_e}{H_i}(1+H_i e)]}\left[x - \frac{(1+H_i e)}{H_i}\right] \tag{34}$$

And the temperature of external surface

$$\theta(0,t) = \sum_{n=1}^{\infty} \gamma_n e^{-ak_n^2 t} + \frac{\varphi_0(1+H_i e)}{\lambda[H_i + H_e(1+H_i e)]} \tag{35}$$

From Eq. (35) h_i cannot be explicitly extracted. However, the temporal evolution of h_i is obtained by identifying the experimental thermogram of the external surface temperature of the rotating cylinder and Eq. (35) at every moment. The evolution of the internal convective coefficient with time is then obtained.

In a steady state, the value of h_i is obtained when t tends towards infinity in Eq. (35) in $x = 0$ (external face), so the convective heat transfer coefficient can be explicitly deduced.

$$h_i = \frac{\lambda\varphi_0 - \lambda^2 H_e\theta_{\max}}{\lambda\theta_{\max}(1+H_e e) - \varphi_0 e} \tag{36}$$

This relation giving h_i in steady state, can be directly obtained using heat resistances. Indeed, combining Eqs. (37) and (38) expressing respectively the heat balance on external and internal surfaces of the cylinder, the same expression from h_i as in (36) is obtained.

$$\varphi_0 = h_e\theta_{x=0} + \frac{\lambda}{e}(\theta_{x=0} - \theta_{x=e}) \quad \text{with } \theta_{x=0} = \theta_{\max} \tag{37}$$

$$\frac{\lambda}{e}(\theta_{x=0} - \theta_{x=e}) = h_i\theta_{x=e} \tag{38}$$

In addition, in a steady state, the relative uncertainty on h_i obtained with this method and for our experimental conditions remains lower than 7.4%.

5. Experimental results

This part presents results of all experiments carried out on the convective heat transfer inside an empty rotating cylinder versus dimensionless parameters connected with the axial flow and the rotational speed. The tests were carried out with a cylinder rotational speed ranging from 4 to 880 rpm ($1.6 \times 10^3 \leqslant Re_r \leqslant 4.7 \times 10^5$) and a variable flow rate varying from 0 to 530 $\mathrm{m^3\,h^{-1}}$ ($0 \leqslant Re_a \leqslant 3 \times 10^4$).

To determine Nu, Re_a and Re_r, physical properties of the fluid are taken at the film temperature, in agreement with the most empirical studies about that sort of problem.

Fig. 5 shows a typical evolution of the external surface temperature of the cylinder versus time. This monotonous evolution increases and tends asymptotically towards the temperature of

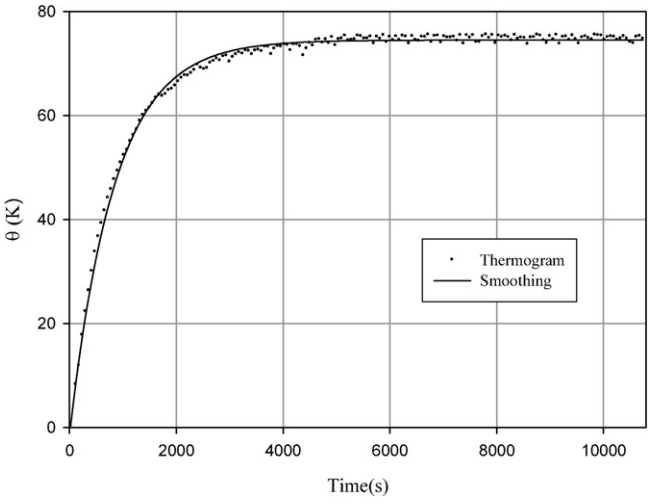

Fig. 5. Typical thermogram on the outer cylinder surface.

thermal balance. This curve is relatively well defined by the following law:

$$\theta = \theta_{\max}\left(1 - \sum_{i=1}^{N} \eta_i e^{-t/\tau_i}\right) \tag{39}$$

Where $\theta_{\max}$ represents the equilibrium temperature, η_i and τ_i are related to the thermogram and numerically obtained for each test.

5.1. Comparison of the models

Values of h_i obtained with the three models developed in this work: inverse technique, isothermal model and analytical model are presented thereafter.

The comparison of the different methods is carried out for the test with the cylinder in rotation at 880 rpm, without any axial airflow and heated with a 2745 W m^{-1} heat flux density. The convective coefficient on the external cylinder surface h_e^{cv} is evaluated using the Dropkin and Carmi correlation [9], Eq. (6). It directly gives $h_e^{cv} = 44.2$ W m^{-2} K^{-1}.

The temperature profile obtained for this operating point presents an increasing exponential evolution well fitted by the following function:

$$\theta = \theta_{\max}\left(1 - \sum_{i=1}^{3} \eta_i e^{-t/\tau_i}\right) \tag{40}$$

with $\theta_{\max} = 17.59K$, and $\eta_1 = 0.426$, $\tau_1 = 0.776$ s, $\eta_2 = 0.425$, $\tau_2 = 644.330$ s, $\eta_3 = 0.275$, $\tau_3 = 80.873$ s.

For the Euler model, the wall of the cylinder is discretized with 11 nodes spaced equally of 0.5 millimeter in the thickness direction. A finer mesh does not significantly change the values of h_i. The time steps adopted for the time discretization is 60 seconds. This time step is chosen equal to the acquisition frequency of the external surface temperatures.

A comparison of the results obtained using the different models is presented on graph 6. It is noted that the three plots relating to the models present almost the same trends. Whatever the identification method used, the initial value of the convective coefficient inside the cylinder is high. This value then gradually decreases and tends towards a limit value identical for all models for large times.

These results also show a good agreement between the different models for $t > 480$ s since for these times, the average relative error remains lower than 8%. However for initial calculation steps ($t < 480$ s) significant differences are to be noted. This can be explained, in the Euler model by the important time step (60 s) which alters the temporal derivative calculation whenever these derivatives strongly change and thus at the initial moments. For the isothermal model, the source of error can come from the isothermal assumption which is not true at the beginning. However the isothermal model gives excellent results for important times and can be quickly implemented. For the analytical model, h_i is assumed to be constant for equations resolution, this assumption can entail inaccuracies at the initial instants.

Table 2
Value of the internal heat transfer coefficients h_i in steady state

$\omega = 880$ tr mn^{-1} $Re_r = 458360$	Isothermal model	Analytical model	Inverse model
h_i [W m^{-2} K^{-1}]	108.31	106.97	104.26

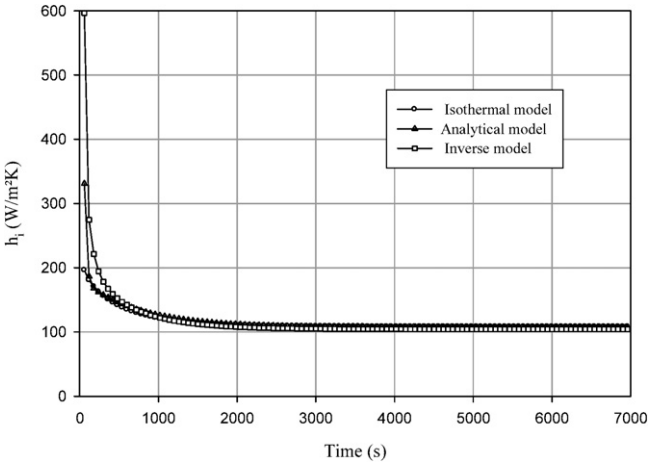

Fig. 6. Evolution of the heat transfer coefficient with time for the different models ($Re_r = 458360$ and $Re_a = 0$).

To calculate the convective coefficient in a steady state, the equilibrium temperature is averaged over the last moments (i.e. the last 600 s). Its variation during this time is about 0.07 K and without significant consequence over the determination of h_i. The values of the convective coefficient h_i obtained in a steady state using the various methods are plotted on Table 2. It is noted that the results are close, and the relative uncertainty does not exceed 4%.

5.2. Validation of the experimental method

The validation of the experimental method is carried out in the case of a cylinder at rest with an axial flow. This configuration is motivated by the existence of many works about the convective heat transfer inside a stationary pipe with an axial flow. To ensure a uniform heating of the external cylinder surface, this cylinder is driven in rotation but at a very low angular speed $\omega = 4$ tr min^{-1} which corresponds to $Re_r = 1731$ and limits the effects of rotation on the values of the convective coefficients. For all the tests the axial Reynolds number ranges from 2737 to 25047.

The influence of the external natural convection is taken into account using the Grashof number. The cylinder temperature in a steady state is used to evaluate the latter. Using Eq. (2) the critical Reynolds number can then be deducted and $Re_c = 23662$. So we are in the case where $Re_r < Re_c$ and the thermal transfer outside the cylinder is thus governed by a mixed convection law. Then Etemad correlation, Eq. (8), is used to estimate the convective heat transfer coefficient and gives: $h_e^{cv} = 7.5$ W m^{-2} K^{-1}.

Fig. 7 presents the experimental thermograms obtained for the various axial airflows. With a constant heating flux, $\varphi_0 = 2185 \pm 10$ W m^{-2}, the increase in the air flow rate involves an

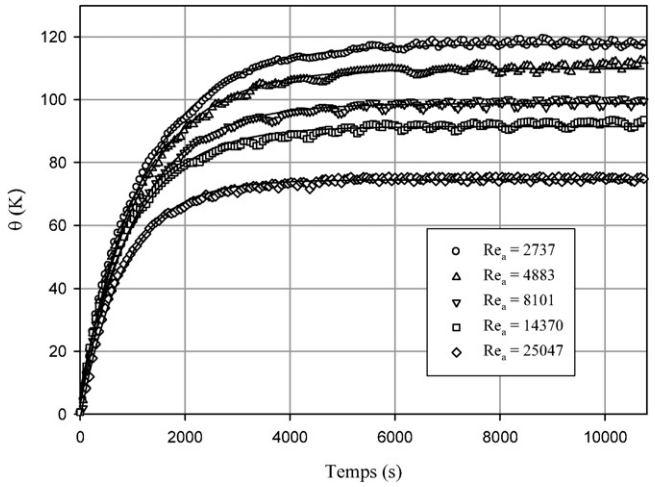

Fig. 7. Temperature time evolution on the cylinder outer surface with an axial air flow.

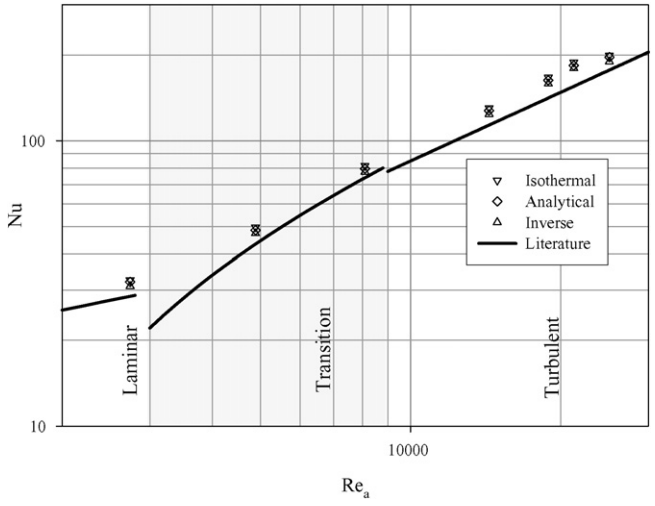

Fig. 8. Evolution of the Nusselt number with axial Reynolds number.

enhancement of the heat transfer between the cylinder and the air flow which results in the reduction in the surface temperature.

Results about the internal convective coefficients are compared with the data of McAdams and Hausen correlated by Eqs. (15)–(17). Those equations are chosen among the other existing works because they are well suited to the conditions of this study. Indeed, this choice is motivated by the dimensions of the cylinder under study which is relatively short ($L/D_i = 0.50$) and the fact that these correlations are mainly well adapted to the inlet tubes regime. The (15), (16) and (17) correlations are valid only in a steady state, thus only the values of h_i obtained for t tending towards infinity are compared hereby. To better appreciate these results we plot on Fig. 8 the evolution of the convective coefficient h_i inside the 4 rpm rotating cylinder for different axial airflows and those resulting from literature. This comparison remains pertinent as long as the axial air flow rate is not too high. Indeed, the connexion cylinder coupled to the low rotational speed insures an airflow close to the one observed in a straight-pipe.

Table 3
Comparison of the results

Re_a	2737	4883	8101	14370	18890	21255	25047
$\varepsilon^{\text{isothermal}}$ [%]	14	14	11	14	18	21	12
$\varepsilon^{\text{analytical}}$ [%]	12	12	8	12	15	18	11
$\varepsilon^{\text{inverse}}$ [%]	8	9	5	9	12	15	7

Table 3 presents the relative error $\varepsilon = |Nu_{\text{exp}} - Nu_{\text{corr}}|/Nu_{\text{corr}}$ obtained between the correlations and the models developed for this study. As we can note, these relative errors are pretty satisfying. Indeed, we note a maximum relative uncertainty equal to 21% between the experimental results and the results obtained using correlations. These variations can be entailed by the cylinder rotation which slightly disturbs the internal air flow and thus tends to increase the heat transfer. These variations can also be explained with the differences between the geometries studied in literature and the geometry of this work. Indeed, in the device studied the inlet axial air flows through several holes whereas in the bibliography the air flows directly through tubes. In this table, the inverse and analytical models produce better results than the isothermal cylinder model with a slight advantage for the inverse method. All in all, the isothermal model is less accurate than other models whatever the axial air flow. This seems coherent since an axial flow promotes the internal face cooling and in that case the isothermal cylinder assumption will be less realistic.

5.3. Rotating cylinder with an axial air flow

Fig. 9 plots the temporal evolution of the convective heat transfer coefficient versus the rotational Reynolds number for various axial Reynolds numbers. Whatever the rotational speed and the axial flow, temporal evolutions of h_i are analogous. In a general way, initially the convective coefficient abruptly decreases. This decrease is followed by an asymptotic behaviour which tends towards a finished limit value corresponding to the steady state and depending both on axial flow and rotational speed. This temporal reduction in the convective coefficient is mainly caused by the increase in the thermal boundary layer thickness. For an imposed air flow rate, an increase in the convective heat transfer coefficient with the rotation can additionally be observed. This is explained by the rotation which generates a destabilizing effect due to the increase in the shear stresses caused by the wall rotation and thus promotes heat exchanges.

Results of tests carried out in a stationary regime were presented on Figs. 10 and 11 as $Nu = f(Re_r)$ and $Nu = f(Re_a)$. As previously observed, it appears clearly that the heat transfer rate increases with rotation. Indeed, the rotation entails a change in the air flow due to the shear effects which enhance heat exchange between the moving wall and the air.

On Fig. 10 for low rotational speeds, the usual results of a static cylinder with an axial air flow are found again: heat transfer increases with the axial air flow. The Nusselt numbers are greater than the values obtained with traditional correlations related to a fixed cylinder and the difference increases whenever

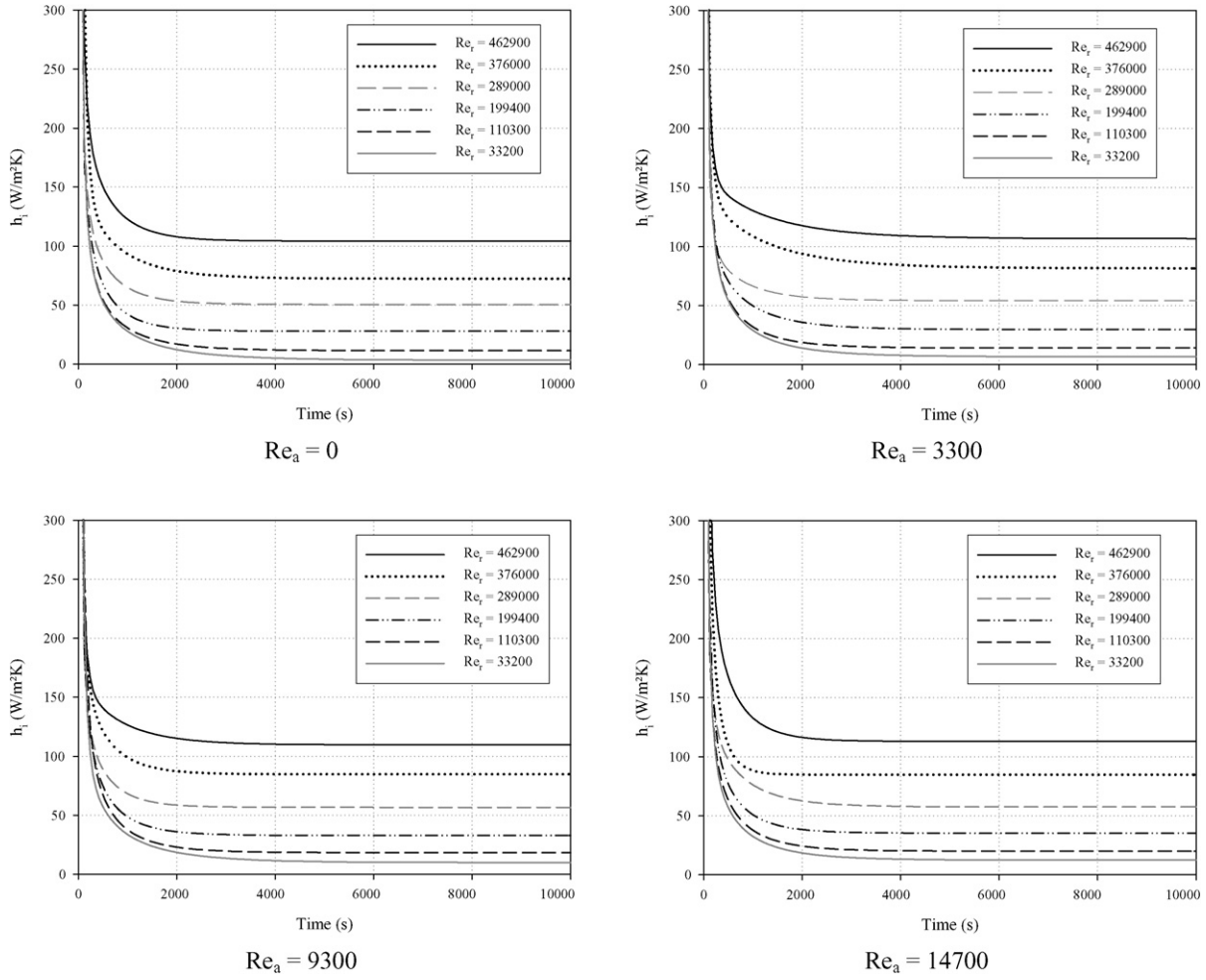

Fig. 9. Temporal evolution of the heat transfer coefficient with the Reynolds number (inverse model).

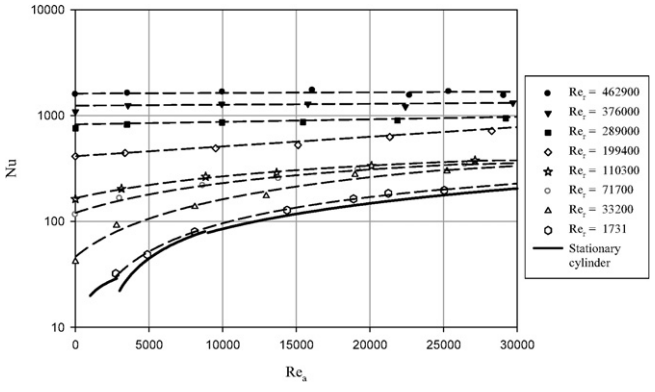

Fig. 10. Evolution of the Nusselt number with Re_a for different rotational speeds.

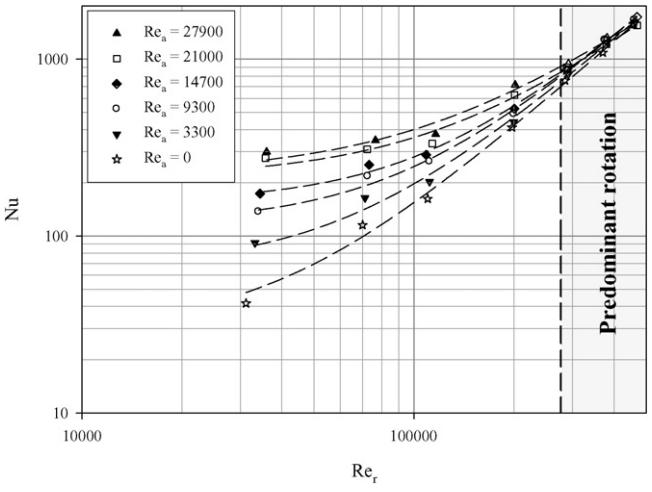

Fig. 11. Evolution of the Nusselt number with Re_r for different flow rates.

the rotational speed increases. However the axial flow is less influenced for the high rotational speed and the convective heat transfer is governed by the rotational Reynolds number.

Fig. 11 shows the existence of two heat transfer regimes. For low rotational speeds, heat transfer increases with axial and rotational Reynolds numbers. When the rotational speed increases, values of the Nusselt number tend towards values almost independent from the axial Reynolds number, which shows the negligible influence of the axial flow on the convective heat transfer. The independence of the convective transfer to the axial flow is characterized on Fig. 11 by the contraction of the different curves. To separate the influence domains, we defined a purely mathematical criterion such that the transition occurs at the points where the difference between the

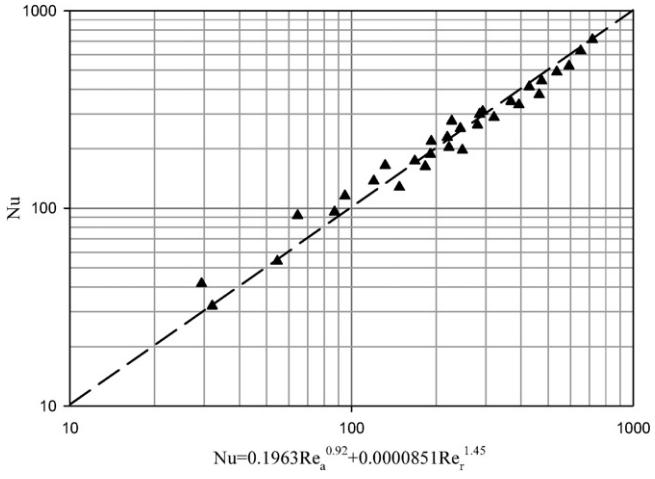

Fig. 12. Comparison of experimental results and obtained correlation (42) for $0 < Re_a < 3 \times 10^4$ and $1.6 \times 10^3 < Re_r < 2.77 \times 10^5$.

curves is minimal. With this aim in mind, we study correlations $Nu_i = f_i(Re_r)$, for each axial flow. From these correlations, we seek the solutions of the following equation:

$$Nu_{i+1} - (1+s)Nu_i = 0 \tag{41}$$

Where s represents the relative difference between the values of the curves Nu_i and Nu_{i+1}.

We admit that the rotation becomes preponderant when the relative difference between curves is lower than 8%. The resolution of Eq. (41) provides the critical rotational Reynolds number Re_r^{crit} from which the convective heat transfer becomes almost independent from the axial flow. The critical value retained is the one which corresponds to the greatest rotational Reynolds number, i.e. $Re_r^{\text{crit}} = 2.77 \times 10^5$.

5.4. Seek of a correlation between the dimensionless parameters

The existing literature does not suggest results in the case of the configuration studied. Using all the results obtained, correlations connecting the convective heat transfer to the rotation and the axial air flow are proposed. Then we seek to correlate experimental points to an equation connecting the inner Nusselt number in a steady state with both the axial and rotational Reynolds numbers. Results about convective heat transfer show we have to consider two flow regimes: the first one for the low rotational speeds, for which the convective heat transfer is governed by both the rotation and the axial flow; the second one for high rotational speeds, for which the convective heat transfer is governed by rotation, and where the axial flow has a weak influence.

For the low values of the rotational Reynolds number ($Re_r < 2.77 \times 10^5$), the heat transfer rate depends both on the axial and rotational Reynolds number. So, we seek a relation such as:

$$Nu = b\,Re_a^c + d\,Re_r^f$$

From the least square method, the following correlation was established, with an average relative uncertainty lower than 11% for the range studied parameters (Fig. 12):

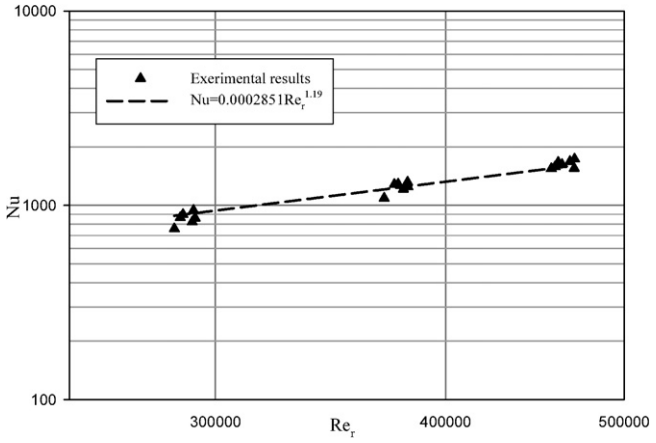

Fig. 13. Evolution of Nusselt number with the rotating Reynolds number ($Re_r > 2.77 \times 10^5$).

$$Nu = 0.01963Re_a^{0.9285} + 8.5101 \times 10^{-6}Re_r^{1.4513}$$
$$0 < Re_a < 3 \times 10^4 \quad \text{and} \quad 1.6 \times 10^3 < Re_r < 2.77 \times 10^5 \tag{42}$$

For greater rotational speeds: $Re_r > 2.77 \times 10^5$, convective exchanges on the internal wall of the cylinder are almost independent from the axial air flow and are completely governed by the effects of rotation. The influence of Re_a on the heat transfer is then negligible. Rotation entails an increase in the convective heat transfers on the internal cylinder surface; the Nusselt number is an increasing function of Re_r, being correlated by Eq. (43). This correlation is established with an average relative uncertainty lower than 5% on the considered domain (Fig. 13):

$$Nu = 2.85 \times 10^{-4}Re_r^{1.19}$$
$$Re_r > 2.77 \times 10^5 \tag{43}$$

6. Conclusion

Infrared thermography allows to identify the convective heat transfer coefficient inside a heated empty rotating cylinder with an axial airflow, for a Reynolds number axial ranging from 0 to 3×10^4 and Reynolds rotational number varying between 1.6×10^3 and 4.7×10^5. Several identification models are developed and tested in order to determine their relevance to evaluate the convective coefficient. They are all based on the knowledge of the external cylinder surface temperature obtained in experiments using infrared thermography. Results obtained for a stationary cylinder are in good agreement with correlations found in literature. The investigations point out the time evolution of the convective coefficient on the internal face of the cylinder. The convective exchanges on the internal wall of the cylinder depend on the rotation and the axial air flow. For high rotational speeds, the heat transfer rate is governed by rotation and the axial flow only slightly influences the internal convective heat transfer. Finally, two correlations providing the Nusselt number are proposed. The first one is relevant for the low rotational speeds and the Nusselt number is a function of both the rotational and axial Reynolds numbers. The second one is relevant for high rotational speeds. In this case the heat transfer rate only depends on the rotational Reynolds number.

References

[1] G.I. Taylor, Stability of a viscous liquid contained between two rotating cylinders, Roy. Soc. London Philos. Transaction Edition A 223 (1923) 289–343.

[2] I.S. Bjorklund, W.M. Kays, Heat transfer between concentric rotating cylinders, J. Heat Transfer 81 (1959) 175–186.

[3] K.M. Becker, J. Kaye, Measurements of diabatic flow in an annulus with an inner rotating cylinder, J. Heat Transfer 84 (1962) 97–105.

[4] W.J. Minkowycz, Y.N. Lee, Heat transfer characteristics of the annulus of two-coaxial cylinders with one cylinder rotating, Int. J. Heat Mass Transfer 32 (4) (1989) 711–722.

[5] C. Gazley, Heat transfer characteristics of the rotational and axial flow between concentric cylinders, J. Heat Transfer 80 (1958) 79–90.

[6] R.E.M. Morales, A. Balparda, A. Silveira-Neto, Large-eddy simulation of the combined convection around a heated rotating cylinder, Int. J. Heat Mass Transfer 42 (1999) 941–949.

[7] I.T. Anderson, O.A. Saunders, Convection from an isolated heated horizontal cylinder rotating about its axis, Proc. Roy. Soc. A. 217 (1953) 555.

[8] G.A. Etemad, Free convection heat transfer from a rotating cylinder to ambient air, with interferometric study of flow, Trans. ASME 77 (1955) 1283.

[9] D. Dropkin, A. Carmi, Natural convection heat transfer from a horizontal cylinder rotating in air, Trans. ASME (1956) 741–749.

[10] W.M. Kays, I.S. Bjorklund, Heat transfer from a rotating cylinder with and without cross flow, Trans. ASME paper N°56-a-71, 1956.

[11] B.A/K Abu-Hijleh, W.N. Heilen, Correlation for laminar mixed convection from a rotating cylinder, Int. Comm. Heat Mass Transfer 25 (6) (1998) 875–884.

[12] K.M. Becker, Measurements of convective heat transfer from a horizontal cylinder rotating in a tank of water, Int. J. Heat Mass Transfer 6 (1963) 1053–1062.

[13] A.A. Kendoush, An approximate solution of the convective heat transfer from an isothermal rotating cylinder, Int. J. Heat Mass Transfer 17 (1996) 439–441.

[14] B. Özerdem, Measurement of convective heat transfer coefficient for a horizontal cylinder rotating in quiescent air, Int. Comm. Heat Mass Transfer 27 (3) (2000) 389–395.

[15] R. Shimada, T. Ohkubo, T. Kobayashi, S. Kumagai, Heat transfer from a rotating cylinder with and without cross flow, Heat Transfer – Japan. Res. 21 (1992) 109–122.

[16] F.W. Dittus, L.M.K. Boelter, Heat transfer in automobile radiators of the tubular type, reprinted in: Int. Comm. Heat Mass Transfer 12 (1985) 3–22.

[17] W.M. Kays, H.C. Perkins, Internal flow in ducts, in: W.M. Rohsenow, J.P. Hartnett (Eds.), Handbook of Heat Transfer, McGraw-Hill Book Company, New York, ISBN 0-07-053576-0, 1973, pp. 7.1–7.193.

[18] F.W. Dittus, L.M.K. Boelter, Univ. of Calif. Pubs Engrg. 2 (443) (1930).

[19] W.H. McAdams, Heat Transmission, McGraw-Hill Book Company, New York, 1954, p. 219.

[20] A.P. Colburn, A method of correlating forced convection heat transfer data and a comparison with fluid friction, Trans. AIChE 29 (1933) 174–210.

[21] L.H. McAdams, Transmission de la chaleur, Dunod, Paris, 1961.

[22] H. Hausen, Darstellung des warmeuberganges in rohren durch verallgemeinerte potenzbeziehungen, Z. VDI Beihefte Verfahrenstechnik 4 (91) (1943).

[23] W.M. Kays, Numerical solutions for laminar-flow heat transfer in circular tubes, Trans. ASME 77 (1955) 1265–1274.

[24] D.G. Kröger, Air-cooled heat exchangers and cooling towers—Thermal-flow performance evaluation and design, Dept. of Mechanical Engineering, South Africa, 1998.

[25] T.J. Pedley, On the instability of viscous flow in a rapidly rotating pipe, J. Fluid Mech. 35 (1969) 97–115.

[26] H.M. Nagib, Z. Lavan, A.A. Fejer, L. Wolf, Stability of pipe flow with superposed solid body rotation, Phys. Fluids 14 (1971) 766–768.

[27] P.A. Mackrodt, Stability of Hagen–Poiseuille flow with superimposed rigid rotation, J. Fluid Mech. 73 (1976) 153–164.

[28] F. Levy, Strömungserscheinungen in rotierenden Rohren, VDI ForschArb. Geb. Ing. Wes. 322 (1929) 18–45.

[29] A. White, Flow of fluid in an axially rotating pipe, J. Mech. Engrg. Sci. 6 (1964) 47–52.

[30] V.K. Shchukin, Hydraulic resistance of rotating tubes, J. Engrg. Phys. 12 (1967) 418–422.

[31] A.I. Borisenko, O.N. Kostikov, V.I. Chumachenko, Experimental study of turbulent flow in a rotating channel, J. Engrg. Phys. 24 (1973) 770–773.

[32] M. Murakami, K. Kikuyama, Turbulent flow in axially rotating pipes, J. Fluids Engrg. 102 (1980) 97–103.

[33] K. Kikuyama, M. Murakami, K. Nishibori, K. Maeda, Flow in an axially rotating pipe, Bull. JSME 26 (1983) 506–513.

[34] M. Murakami, K. Kikuyama, K. Nishibori, Three dimensional boundary layer development in an axially rotating pipe, in: Proc. 3rd Symp. Turbulent shear flows, Calif. Univ. 2.1–2.6, 1981.

[35] K. Kikuyama, M. Murakami, K. Nishibori, Development of three-dimensional turbulent boundary layer in an axially rotating pipe, J. Fluids Engrg. 105 (1983) 154–160.

[36] S. Imao, M. Itoh, T. Harada, Turbulent characteristics of the flow in an axially rotating pipe, Int. J. Heat Fluid Flow 17 (1996) 444–451.

[37] G. Reich, Strömung und wärmeübertragung in einem axial rotierenden Rohr, Doctoral Thesis, TH Darmstadt, 1988.

[38] G. Reich, B. Weigand, H. Beer, Fluid flow and heat transfer in an axially rotating pipe—II. Effect of rotation on laminar pipe flow, Int. J. Heat Mass Transfer 32 (3) (1989) 563–574.

[39] J.N. Cannon, W.M. Kays, Heat transfer to a fluid flowing inside a pipe rotating about its longitudinal axis, J. Heat Transfer 91 (1969) 135–139.

[40] G. Reich, H. Beer, Fluid flow and heat transfer in an axially rotating pipe—I. Effect of rotation on turbulent pipe flow, Int. J. Heat Mass Transfer 32 (3) (1989) 551–562.

[41] B. Weigand, H. Beer, Fluid flow and heat transfer in an axially rotating pipe subjected to external convection, Int. J. Heat Mass Transfer 35 (7) (1992) 1803–1809.

[42] I.E. Idel'cik, Memento des pertes de charges, Collection de la direction des études et recherches d'Électricité de France, Éditions Eyrolles, Paris, 1969.